Regular Article

PHYSICAL CHEMISTRY RESEARCH
Published by the
Iranian Chemical Society
www.physchemres.org
info@physchemres.org

Phys. Chem. Res., Vol. 9, No. 2, 261-279, June 2021
DOI: 10.22036/pcr.2021.257129.1853

A Comprehensive Study on Synthesis Parameters of TiO_2 Nanotube Arrays: The Effects on Morphology and Photocatalytic Degradation of Para-NitroPhenol

N. Rahimpour[a], M. Mollavali[b,*] and F. Rashidi[a]

[a]*Department of Chemical Engineering, Amirkabir University, Tehran, Iran*

[b]*Department of Chemical Engineering, Faculty of Engineering, Ardakan University, P. O. Box: 184, Ardakan, Iran*

(Received 13 November 2020, Accepted 6 February 2021)

The present research aimed to evaluate the effects of synthesis parameters on morphology and photocatalytic activity of TiO_2 nanotube aligned arrays (TNAs) *via* a low-cost anodization process. The impact of electrolyte composition, anodization time, and applied voltage on morphological and architecture properties of TNAs, including length, inner diameter and wall thickness, were accurately investigated. We further studied the effect of heat treatment on crystalline and phase transformation of the samples at different annealing temperatures. Photocatalytic properties of the fabricated samples were studied for degradation of p-nitrophenol under UV light irradiation. The physicochemical characteristics of the photo-anodes were observed using several techniques including field emission scanning electron microscopy, energy dispersive X-ray spectroscopy and XRD. Moreover, the maximum photocatalytic performance for p-nitrophenol degradation was obtained as about 80%.

Keywords: Anodization, Synthesis parameters, TiO_2 Nanotubes, Morphology, *P*-nitrophenol degradation

INTRODUCTION

Industrial Revolution has been followed by many environmental problems such as increasing in organic pollutants content in water [1]. Therefore, selection of the best methods for treating of wastewater from different industries is very important. One of the effective techniques in wastewater treatment is photocatalytic technology [2-6]. Over the past decade, many investigations have been performed on development of photo-electrochemical devices composed of suitable photocatalysts for degradation of organic pollutants under simulated sunlight irradiation.

Among various photocatalytic systems, some nanomaterials have been used as photocatalysts in forms of nanotube [7,8], nanorod [9] and nanoparticle [10,11]. However, more efforts have been made on nanotubes [12], due to their benefits such as high efficient absorption of collision photons as well as transmission photogenic electrons.

*Corresponding author. E-mail: mollavali@ardakan.ac.ir

Furthermore, among the numerous types of semiconductors, TiO_2-nanotubes prepared by electrochemical anodization of titanium foil have attracted more attention, due to their special features and benefits including high photo-electrochemical stability, ease of scale-up, non-toxicity, chemical inertness, good recyclability, excellent photocatalytic activity, high surface area, and low cost [13,14]. Raja *et al.* [15] used an anodization process to synthesize the TiO_2 nanotubes in an ethylene glycol-based solution with 0.2% NH_4F, different amounts of water concentration, at 20 V constant voltage for 45 min. Their results demonstrated that 0.18 wt% of water content is required to fabricate a regular TiO_2 nanotube arrays.

Wan *et al.* [16] evaluated the effects of NH_4F concentration, H_2O content, oxidation time and anodization voltage on the length of nanotubes and reported the best values of anodization parameters to fabricate nanotubes with 45 μm in length (pore diameter of about 100 nm). Vaenas and his group [17] investigated the effects of calcination temperature, calcination time and heating rate on

phase transformation and crystallinity of anodized TiO_2 nanotubes. Thabit *et al.* studied the effects of several aqueous electrolytes to control the dimensions of the anodic TiO_2 nanotube arrays [18]. The effect of anodization time and applied voltage were also studied by Chernozem *et al.* [19]. They reported that the nanotube length varies from 1410 nm to 6270 nm, when anodization time increases from 0.5 to 4 h at a constant voltage of 60 V. The effects of voltage and anodization temperature, in an ethylene glycerol-based electrolyte containing 0.38 wt% NH_4F and 1.79 wt% H_2O are investigated by Sulka *et al.* [20]. The effect of water content in ethylene glycol-based electrolyte was studied by Sun *et al.* [21]. Their results revealed that the anodized sample with 2 wt% water content in electrolyte can produce the highest amounts of hydrogen in water splitting reaction. Variation in tube length and diameter with increasing in ethylene glycol content is another research topic examined by Song *et al.* [22]. They successfully achieved a photocatalytic efficiency of about 95% for degradation of Rhodamine under visible light irradiation. Some research activities focused on modification of TiO_2 nanotube arrays with other semiconductors/sensitizers to increase the light harvesting. The results have been used in the photocatalytic degradation of organic pollutants such as p-nitrophenol [23,24].

Therefore, studying the structural modification of pure TiO_2 nanotube arrays by variation of synthesis parameters could be of crucial importance. However, to the best of our knowledge, there are very few reports on photocatalytic degradation of *p*-nitrophenol (as an organic pollutant) using TiO_2 nanotube arrays (TNAs) under UV-LED irradiation. Here, the effects of independent variables including anodization time, water and ammonium fluoride content, and applied voltage on structural morphology and photocatalytic performance of fabricated TNAs are systematically investigated. At the end, the impact of annealing temperature (as an independent factor) on crystallinity and photo-catalytic activity of samples is studied. Morphology of the samples is also investigated using a simple geometrical model.

MATERIALS AND METHODS

Titanium foils with a 0.8 mm wall thickness (99.6% purity), and all chemical materials were purchased from Alfa-Aesar (Ward Hill, MA, USA) and Merck. Briefly, prior to anodization, the titanium foils were cleaned and degreased by sonicating, for 45 min in ultra-pure water, acetone and finally ethanol, followed by rinsing with distilled water, and then dried off in a flowing air stream. Then, as-prepared titanium foils were chemically etched by immersing in a mixture of 3.2 M HF and 5.5 M HNO_3 for 20 s, and immediately rinsed again with deionized water, dried under an air stream and used immediately. Anodic oxidation experiments were conducted by potentiostatic anodization in a conventional dual-electrode electrochemical chamber, as shown in Fig. 1. After pretreatment, the polished Ti sheet (2×4 cm^2) was used as a working electrode and a titanium rectangular foil with a size of 5×5 cm^2 was served as a counter electrode. The Ti sheet with an active anode area of about 5 cm^2 was kept between a set of O-rings in a sample holder, and a copper wire was connected to both anode and cathode as the electrical contact. The anodization was performed in an ethylene glycol based electrolyte containing different amounts of NH_4F (0.1-0.4 wt%) and H_2O (1.2- 40 wt%), at different durations of 30 min, and 3, 6, 9, 12 h, using various voltages (10-45 V). Both electrodes (cathode and anode) with a distance of 3 cm were placed in a Teflon vessel and the potentiostatic anodization experiments were conducted using one factor/variable at a time technique at room temperature. A DC power supply (MEGATEK MP-3005D, Taiwan) was used as a voltage source to handle time-dependent anodization current tests. As shown in Fig. 1, two distinct/separated chambers were employed and connected to DC power supply to fabricate two different samples simultaneously. After electrochemical anodization process, the fabricated electrodes were rinsed properly with ultra-pure water for a couple of minutes to avoid dissolution of TNAs and to remove the occluded ions, and subsequently dried in an air stream. In order to enhance the adhesion force between TiO_2 layers with substrate and also to remove any surface debris, the electrodes were annealed at 100 °C for 30 min, and then sonicated for 5 min in doubly distilled water. As-prepared electrodes then were calcined in air environment for 100 min at different temperatures (300-700 °C) with heating and cooling rates of 1°C min^{-1} to transform the amorphous titania into nanocrystalline anatase.

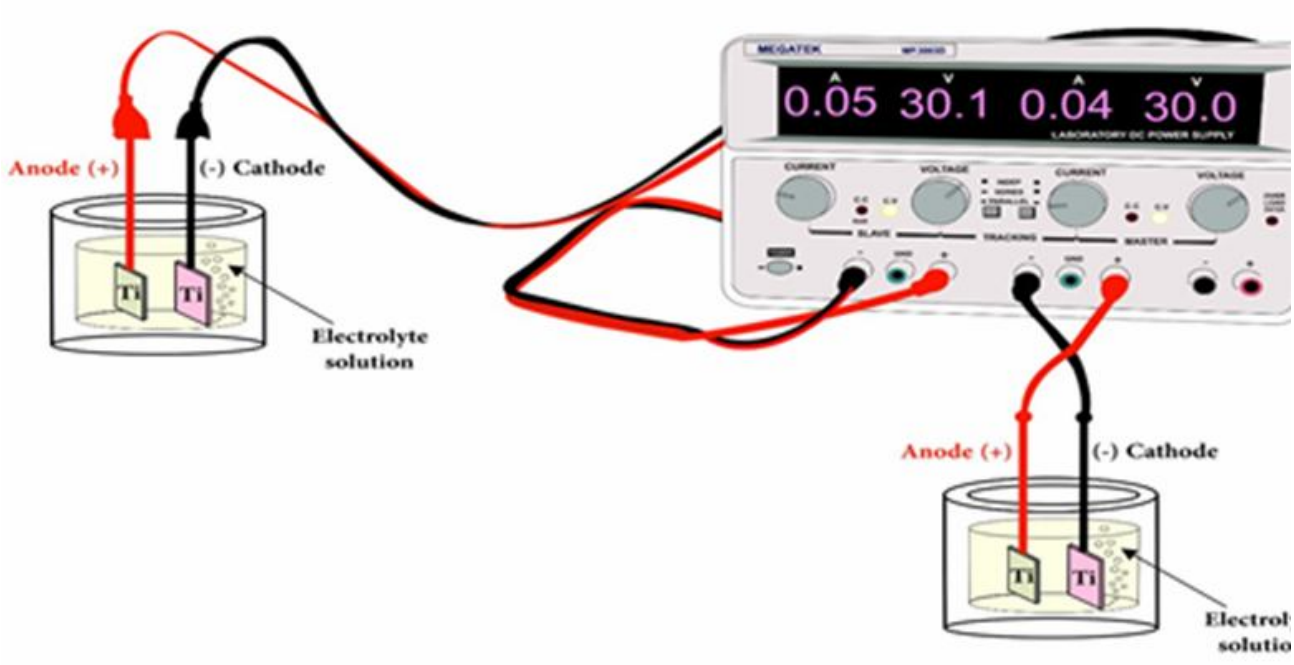

Fig. 1. Schematic diagram illustrating the anodization setup for TNAs synthesize.

Physical and Chemical Characterization Techniques

Surface morphology of the as-prepared photo-electrodes was recorded through field emission scanning electron microscopy (FE-SEM) using a Hitachi, S-4800 Field Emission SEM apparatus equipped with a PulseT or Maxim/Quartz Imaging XOne EDX system. The elemental composition of the photo-anodes was determined by EDX analysis. The crystal structure and phase composition/identification of the semiconductors were examined by X-ray diffraction diffractometer (Rigaku RINT 2500, Tokyo, Japan) with Cu Kα radiation (λ = 1.54059 Å), at 40 kV and 50 mA over a 2θ range from 20°-80° with a step width of 0.02° s^{-1}. Specific surface area (SA), surface roughness factor (G) and porosity of the synthesized semiconductors were calculated using the following equations [25-28]:

$$SA = \frac{4}{\pi D_0^2} \times \pi[D_i L + (D_0^2 - D_i^2)] = \frac{4[D_i L + (D_0^2 - D_i^2)]}{D_0^2} \quad (1)$$

$$Porosity = 1 - \frac{2\pi W(W + D)}{\sqrt{3}(D + 2W)^2} \quad (2)$$

$$G = \frac{4\pi L(W + D)}{\sqrt{3}(D + 2W)^2} + 1 \quad (3)$$

where L is nanotube length (μm), D_i and/or D display inner diameter (nm) and D_o represents outer diameter of TiO_2 nanotubes (nm), respectively. The above-mentioned factors were developed using a simple geometrical model. Assuming an ideal regular network of identical, equally spaced and hexagonally arranged nanotubes (a single regular hexagon with one pore inside), specific surface area of the fabricated TNAs (as a dimensionless parameter) can be estimated by sum of the inner cylindrical and flat top side surface area of the nanotubes divided by nanotube density (the total number of nanotubes occupying a unit area of 1 cm^2) [25]. Porosity (%) expresses the ratio of the TiO_2 surface area forming the nanotubes with respect to the sample total surface area [27]. The geometric surface roughness factor (G, as a dimensionless parameter) exhibits the ratio of the cylindrical (inner and outer) and flat (top and bottom) surfaces of the tube arrays relative to the corresponding projected area [27]. Although the geometrical factors were derived from an idealized hexagonal structure when the tubes are close packed, they can be expanded for

the similar structures (quasi-ideal) with negligible error [26].

Photocatalytic Degradation of PNP and Analytical Procedure

The photocatalytic properties of the prepared samples were studied for photodegradation of p-nitrophenol (PNP) in aqueous solution under UV-LED irradiation (NCSU033B (T), NICHIA Co., Japan) with peak emission wavelength of 365 nm. All the experiments were conducted in a photoreactor constructed by a Plexi glass material with a total volume of 100 ml, at ambient temperature. The light intensity on the surface of photoanodes was measured by a UV light meter (Lutron, model 340A, Taiwan) to be 2 mW cm^{-2}. Prior to irradiation, the aqueous solution (initial PNP concentration of 20 mg l^{-1}) was stirred in the dark for 30 min to establish the adsorption-desorption equilibrium of p-nitrophenol on the photocatalyst surfaces as well as a right estimation of PNP removal efficiency in a dark system [29]. Then, the photocatalytic degradation started under light irradiation. Photocatalytic activity of the electrodes for PNP degradation was evaluated by measuring the absorbance at λ_{max} = 400 nm using a single-beam spectrophotometer (SpectroDirect, Model 712000, Loviband Co., United Kingdem).

RESULTS AND DISCUSSION

SEM Results

Figure 2 shows the FE-SEM images of anodized TNAs in various synthesis conditions. As shown in Figs. 2a and c, the surface morphology of TNAs transformed severely by increasing the water content in electrolyte containing of 0.35 wt% NH_4F, at 30 V for 3 h. As a result, inner diameter of tubes increased with increasing the water content. Furthermore, the ripples appeared on the nanotube walls and the length of tubes decreased when water content in electrolyte increased from 1.2 to 40 wt% (Figs. 2b and d). According to Figs. 2e and g, increasing the anodization time increases slightly inner tube diameter and wall thickness, indicating that they are independent of anodization time when the other anodization parameters including water content, time and voltage are kept constant. Also, the length of tubes changes from 9.4 to about 13.5 μm when the anodization time increased from 6 to 12 h, the experimental results are in accordance with other research works (Figs. 2f and h) [30]. No nanotubes were fabricated at 10 V, while highly ordered, circular shape TNAs were formed at the voltages higher than 15 V (see Figs. 2i-k). Furthermore, inner diameter and length of nanotubes increased by increasing voltage, while wall thickness increased slightly with increasing voltage. Referring to Fig. 2l, surface morphology of anodized TNAs with 0.1wt% NH_4F exhibits sponge-like properties, while highly ordered, long tubular structure was synthesized using 0.4 wt% of NH_4F content in ethylene glycol-based electrolyte. The tube inner diameter increased by increasing the NH_4F content in electrolyte, whereas the tube length and wall thickness turned from approximately 4.9 to 5.9 μm and 10.5 to 11.5 nm, respectively, as NH_4F concentration increased from 0.2 to 0.4 wt% (Figs. 2m-o).

To get the right and exact calculation for geometrical model, we selected and scanned different parts of each sample (at least 5 different points of the sample's surface).Many images were taken using FE-SEM apparatus, just a few of them were used in Fig. 2.

The average of tube diameter, tube length and tubes per square unit of area were obtained through the as-mentioned FE-SEM images, and the macroscopic surface area was measured with a ruler added to the FE-SEM apparatus as a software [26].

Energy Dispersive X-ray Spectroscopy (EDX)

Table 1 reveals the EDX results to analyze the elemental composition of the anodized samples at different synthesis conditions, the photo-electrodes were gold sputtered before EDX analysis. This led to eventual appearance of Au peaks in the due diagrams, not present in the original photo-anodes. According to Table 1, high grade TNAs were fabricated at various conditions. Note that, C, F, N and Cu can originate from the precursor solution and/or titanium foil impurities. Also, contaminants (in the form of heteroatoms) can come from the different parts of anodization apparatus and/or characterization equipment such as FE-SEM/EDX, *etc.* [31]. The undesirable incorporation of contaminants (no dopants) may have a negligible effect just in visible part [13,31]. As mentioned before, all the photoactivity experiments were performed

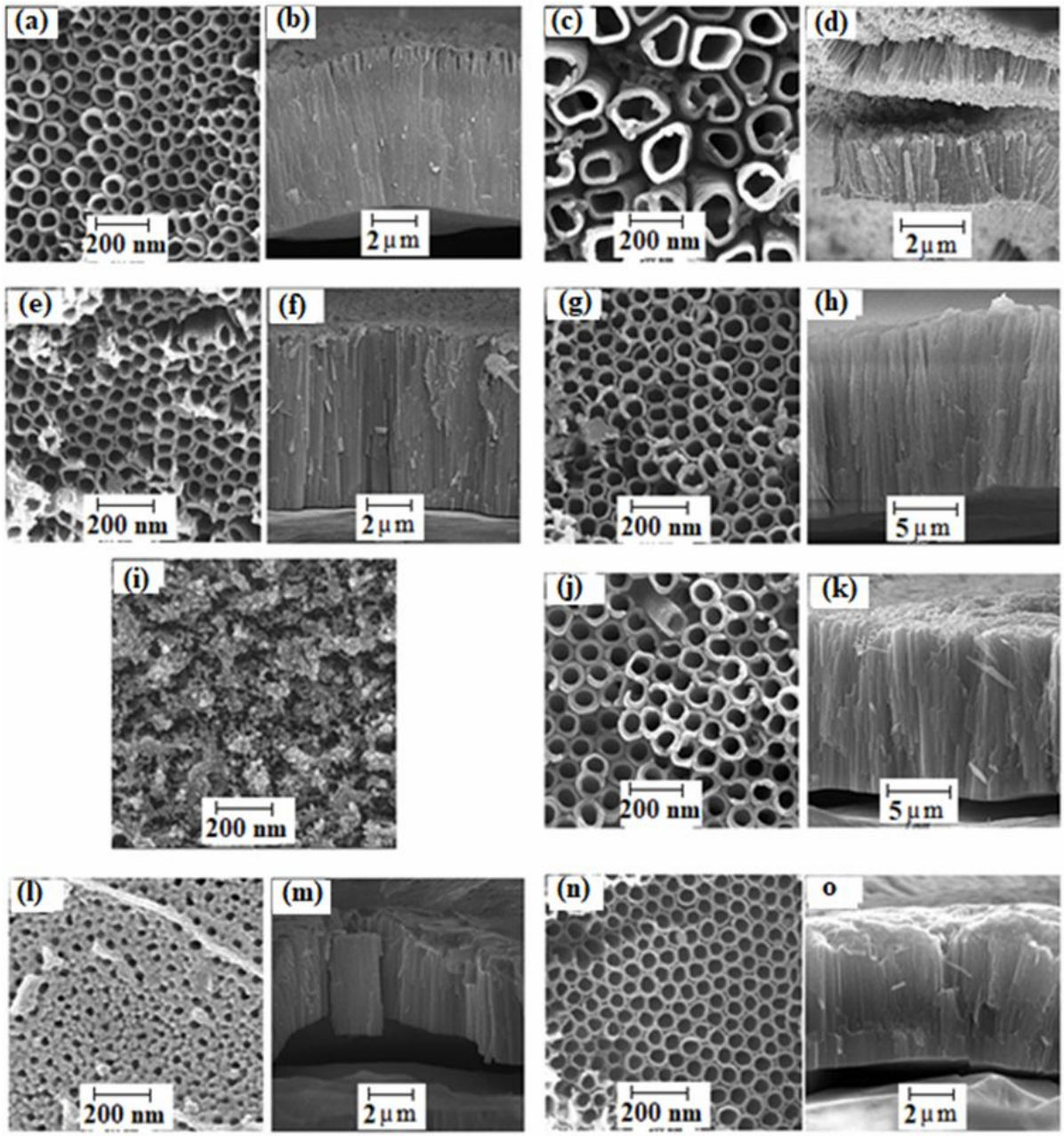

Fig. 2. FE-SEM images of fabricated TNAs under various anodization conditions: (a,c) top views for the effect of 1.2 wt% and 40 wt% of water content in an electrolyte containing 0.35 wt% NH_4F and ethylene glycol, at 30 V for 3 h, (b,d) cross- section, (*e,g.*) effect of anodization time, 6 and 12 h, on an ethylene glycol based-electrolyte consisting of 0.35 wt% NH_4F and 2 wt% water under 30 V (top view of FE-SEM images), (f,h) cross-section, (i,j) top view of FE-SEM images for the effect of voltages at 10 and 45 V (NH_4F concentration: 0.35 wt%, water content: 2 wt%, for 3 h), (k) cross-section; top views for the effect of NH_4F concentration including 0.1 wt% and 0.4 wt% in an ethylene glycol based-electrolyte containing 2 wt% water at 30 V for 3 h (l,n), and (m,o) cross-sectional images.

Table 1. EDX Analysis of Fabricated Samples Using Different Anodization Conditions

Component / Anodization condition	C (wt%)	N (wt%)	O (wt%)	F (wt%)	Au (wt%)	Ti (wt%)	Cu (wt%)	O/T Molar ratio
Water: 1.2 wt%	2.14	2.82	32.62	13.02	0.31	42	0.1	1.99
Water: 10 wt%	1.97	2.39	30.86	9.74	0.33	54.61	0.1	1.69
Water: 20 wt%	1.86	2.15	29.65	7.22	0.34	58.79	-	1.51
Water: 30 wt%	1.64	1.87	28.45	6.98	-	61.06	0.1	1.394
Water: 40 wt%	1.43	1.69	27.33	6.82	-	62.63	0.1	1.31
NH4F: 0.1 wt%	N/A[a]	N/A[a]	N/A[a]	N/A[a]	N/A[a]	N/A[a]	N/A[a]	N/A[a]
NH4F: 0.2 wt%	2.28	2.71	29.18	12.46	0.26	53.12	-	1.64
NH4F: 0.3 wt%	1.93	2.89	32.4	13.01	0.25	49.52	-	1.95
NH4F: 0.4 wt%	1.88	2.96	31.58	13.28	0.28	50.02	-	1.88
Time: 0.5 h	2.91	1.61	26.63	11.22	-	57.63	-	1.38
Time: 3 h	2.58	1.94	29.62	10.94	0.78	54.14	-	1.64
Time: 6 h	2.4	2.8	31.3	10.86	0.91	51.74	-	1.81
Time: 9 h	2.31	2.74	32.06	11.45	0.82	50.62	-	1.90
Time: 12 h	2.27	2.57	32.51	12.1	0.86	49.69	-	1.96
Voltage: 10 V	1.46	1.46	25.72	8.43	-	62.93	-	1.22
Voltage: 17.5 V	2.04	1.69	26.97	9.18	-	60.12	-	1.34
Voltage: 25 V	2.33	1.92	27.58	10.13	-	58.04	-	1.42
Voltage: 35 V	2.47	2.45	31.86	9.57	-	53.65	-	1.78
Voltage: 45 V	1.3	2.76	34.24	7.79	-	53.91	-	1.9

[a](N/A): Not applicable, because no nanotubes were observed at this condition.

under UV (< 365 nm) irradiation.

Impact of Anodization Parameters on Structural Morphology and Photocatalytic Activity of the Synthesized TNAs

The effects of synthesis parameters consisting of water and ammonium fluoride content in electrolyte, anodization time, and applied voltage on photocatalytic activity of anodized samples were widely studied and investigated, to achieve a more in-depth understanding of structural modification. All the experiments for anodization process as well as photocatalytic degradation were carried out under ambient conditions, and performed in triplicate. The percentage of PNP photo-degradation (%) was calculated by the following equation:

$$PNP\ removal\ (\%) = \frac{(Abs_0 - Abs_t)}{Abs_0} \times 100 \quad (4)$$

where Abs_0 displays the initial/original absorbance of PNP solution and Abs_t represents the absorbance of PNP solution irradiated for 60 min, using the fabricated photocatalysts.

Effect of Water Content

Figure 3 reveals the impact of water content in an ethylene glycol based-electrolyte on inner diameter, length, and wall thickness of the fabricated TNAs as well as their photocatalytic performance for PNP degradation. The effect of water content experiments was conducted using 1.2, 10, 20, 30 and 40 wt% water in an electrolyte containing 0.35 wt% NH_4F + ethylene glycol under an applied voltage of 30 V for 3 h. Then, the synthesized samples were calcined at 400 °C for 120 min. In general, the overall reactions for anodization process of Ti can be described as follows [13,21]:

$$Ti + 2H_2O \rightarrow TiO_2 + 4H^+ + 4e^- \quad (5)$$

$$TiO_2 + 6F^- + 4H^+ \rightarrow TiF^{2-}_6 + 2H_2O \quad (6)$$

The initial reaction for anodic oxidation of titanium foil (Eq. (5)) can be described by the following chemical reactions:

$$2H_2O \rightarrow O_2 + 4e^- + 4H^+ \quad (7)$$

$$Ti + O_2 \rightarrow TiO_2 \quad (8)$$

High viscosity of electrolyte and lack of hydrogen ions (H^+) which occur in the absence of water molecules lead to formation of just TiO_2 layers [32]. That is why, a few amounts of water can help to organization and preliminary development of nanotubular structures. At the initial stage, in the presence of lower amounts of water, a thin barrier oxide layer was formed on the titanium foil through electrochemical anodic oxidation of Ti to TiO_2, where field-assisted dissolution dominates chemical dissolution (large electric field across the thin oxide layer). In the next step (Eq. (6)), the formation of small pits and chemical dissolution of the titanium dioxide occur by F^- ions which they are transferred faster in water. Thereafter, small pits convert into the bigger pores. The pores cover and spread over the barrier oxide layer, and then pore growth begin and transform into a highly-ordered tubular structure. Meanwhile, this positive effect of water content in enhancing smoothness and tube length is converted to a negative impact, when the water content in electrolyte increases to higher amounts. This phenomenon can be explained by faster corrosive speed of fluoride ions, where F^- ions enter into the TNAs easily and then attack to the weak points of TNAs [32]. Accordingly, the first-formed TNAs approximately are corroded and consequently prevent the formation of aligned, long and smooth TiO_2 nanotubes (see Fig. 3a, Figs. 2b and d). It means that increasing the water content increases the chemical dissolution (Eq. (6)) compared with the oxidation process (Eq. (5)) [21].

As seen in Fig. 3a, the lengths of tubes obtained with 1.2, 10, 20, 30 and 40 wt% water were 8.25, 6.74, 2.49, 2.3 and 2.2, respectively. Also, the inner diameter of tubes increased from approximately 53 to 112 nm when the water concentration varied from 1.2 to 40 wt%. Both inner diameter and length changed very slowly, when we used water content higher than 20 wt%. This is due to the fact that a part of fabricated TNAs is converted to the porous structure [21]. But the wall thickness slightly elevated within the range of 19-26 nm. The experimental data and observations are in agreement with other research works [33,34].

Geometrical properties including specific surface area (SA), porosity and geometric roughness factor (*G*) of as-prepared TNAs were further investigated. This evaluation was performed through the combination of experimental data obtained from FE-SEM images and Eqs. ((1)-(3)). Table 2 shows the geometrical parameters of the synthesized TNAs with different water contents determined by FE-SEM analysis. As shown in Table 2, the actual active specific surface area (SA) decreased with increasing the water content of ethylene glycol-based electrolyte. Based on Eq. (1), the total active surface area of nanotubes is mainly affected by the tube length as well as the square values of outer diameter [26,35]. Therefore, a decrease in SA is expected with an increase in water content which leads to shorter nanotubes with bigger outer diameter.

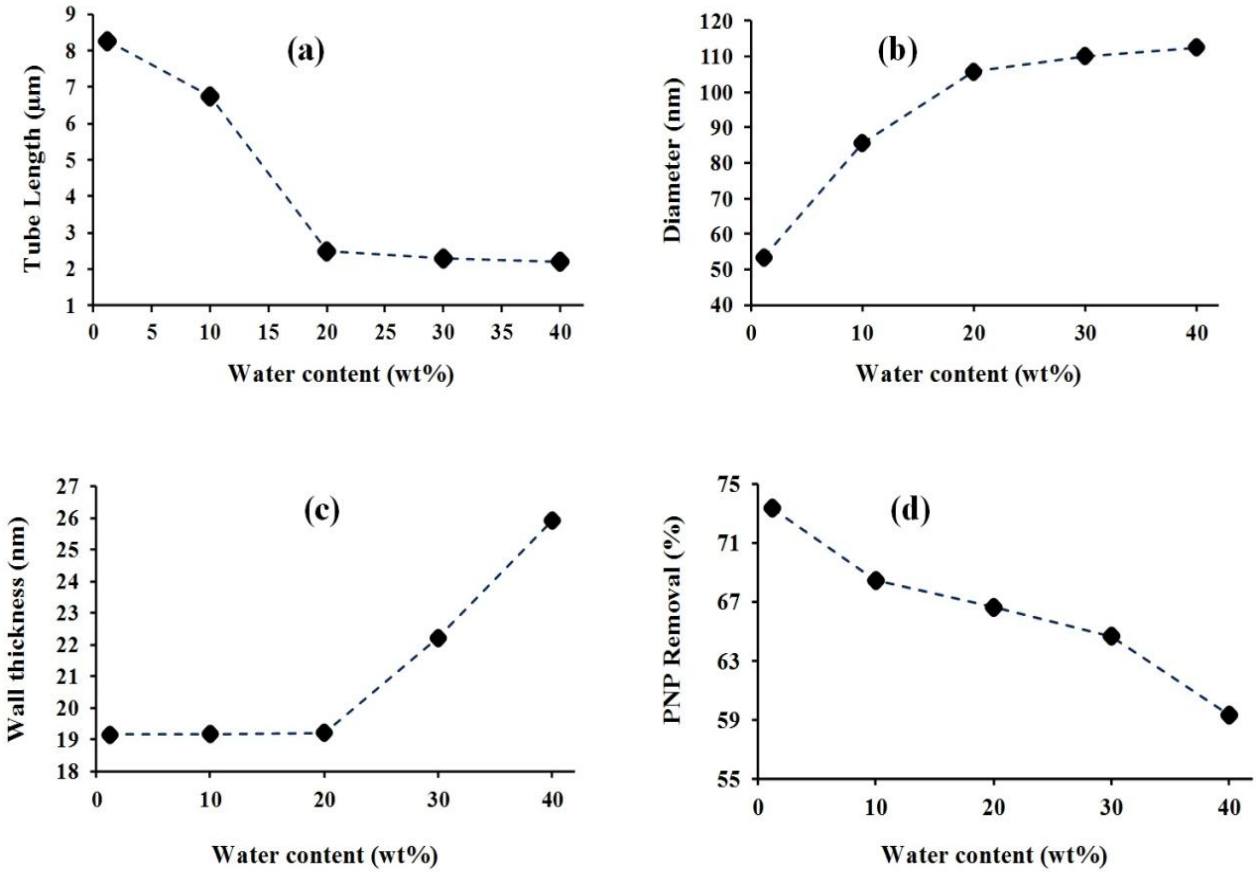

Fig. 3. Influence of water content on length (a), inner diameter (b) and wall thickness (c) of TNAs (an electrolyte containing 0.35 wt% ammonium fluoride + ethylene glycol (EG) at 30 V for 3 h) and their photocatalytic degradation of PNP (d).

Table 2. Geometrical Properties of TNAs Fabricated by Different Amounts of Water

Properties / Condition	Estimated surface area	Estimated roughness factor	Estimated porosity
Water content: 1.2 (wt%)	212.39	516.70	0.40
Water content: 10 (wt%)	152.3045	333.29	0.52
Water content: 20 (wt%)	52.50	108.53	0.58
Water content: 30 (wt%)	44.26	92.13	0.55
Water content: 40 (wt%)	38.90	82.02	0.51

As shown in Table 2, porosity of samples was firstly increased and then slightly decreased by increasing the water concentration in electrolyte. The porosity of photoanodes represents the ratio of TNAs surface area to photo-electrode total surface area including circular openings as well as inner-tube voids [26,28]. According to Eq. (2), porosity of samples is mainly changed by the square amounts of outer tube diameter (see Figs. 3b and c). Photocatalytic activity of fabricated electrodes directly depends on their surface area and porosity, where more adsorption of aqueous reactants occurs using the samples with higher SA. The fabricated photoanodes with higher values of porosity can elevate and control diffusion rate of reactants/ pollutant molecules inside the surface as well as improve light penetration during the photo-reaction (Table 2 and Fig. 3d) [25,27,36].

Based on above discussion, it can be concluded that the photo-activity of the synthesized samples is not only dependent to their SA and porosity, and further investigations are required with other geometrical factors which they have noticeable impact on the photo-activity of TNAs. The geometric surface roughness factor (G), developed to investigate the influence of anodization parameters on geometrical characteristics of fabricated TNAs, represents the ratio of the inner and outer diameters as well as flat top and bottom surfaces of TNAs in comparison with the corresponding anodized area. G factor of the photoanodes is mainly affected by inverse square values of inner/outer tube diameter and also length of tubes (see Eq. (3) and Figs. 3b and 3c). Increasing of water content decreased the roughness factor of anodized samples, due to the formation of bigger nanotubes in diameter as well as shorter tubes. The samples with higher G values indicate that nano tubular structure supports an extended real surface area.

According to Fig. 3d, photocatalytic performance of electrodes, in terms of PNP photo-degradation, decreased from approximately 75 to 60%, when the water concentration increased from 1.2 to 40 wt%. This photocatalytic behavior can be readily explained in terms of their morphology, where photoanodes with higher values of SA and G factor represent better reactivity. It means that, highly regular nanotube arrays with straight, smooth pores and little surface debris display a higher photocatalytic activity.

Effect of Anodization Time

One of the effective parameters on morphological properties of TNAs is anodization time. For glycol-based electrolyte, structural morphology of TNAs is mostly time-dependent (in contrast with water-based electrolyte) [37]. Figure 4 illustrates the structural properties and photocatalytic performance of fabricated TNAs as a function of anodization time. The experiments were performed in an ethylene glycol-based electrolyte containing 0.35 wt% NH_4F and 2 wt% of water under applied voltage of 30 volts for 0.5, 3, 6, 9 and 12 h (calcination temperature and time were kept 400°C and 2 h, respectively). Figure 4a reveals that increasing of anodization time affected on nanotube length and they varied from approximately 2.4 to 13.5 μm when anodization time increased from 0.5 to 12 h. The formation of longer TNAs by elevation of anodization time can be explained by continuous oxidation of Ti sheet to form oxide layer [25,38]. The anodization time also showed a negligible effect on wall thickness, while wall thickness is a time-independent variable. However, inner diameter of tubes increased by increasing the anodization time up to 6 h, and after that remained constant. This phenomenon is mainly due to the continuous chemical dissolution of oxide layer [38].

It was also found that the photocatalytic performance of fabricated TNAs increases by increment of anodization time up to 9 h, and after that decreases dramatically. It could be due to the fact that the geometrical parameters in terms of SA, porosity and G factor show an enhancement with increasing anodization time (see, Table 3). The samples with higher values of G, SA and porosity represent a better photocatalytic performance, as discussed earlier. It should be mentioned that the lower photoactivity of the synthesized sample within 12 h is probably due to the limited depth of incident photon penetration through the nanotubes and diffusion of pollutant molecules into TNAs [36].

Effect of Applied Voltage

The impact of anodization voltage on inner tube diameter, length, wall thickness and photocatalytic performance of fabricated TNAs under UV-LED irradiation,

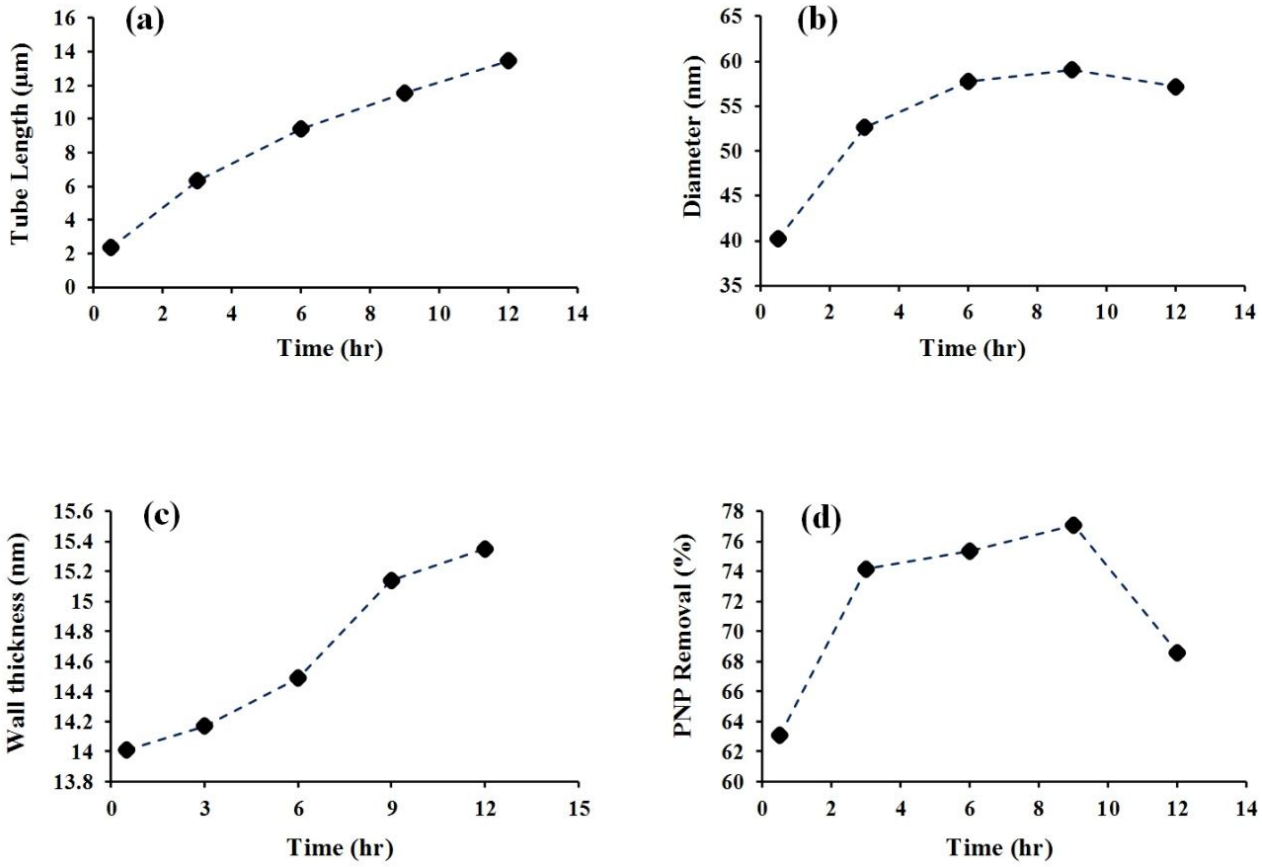

Fig. 4. Variation of length (a), inner diameter (b), wall thickness (c) and photocatalytic performance (d) of fabricated TNAs as a function of anodization time. Anodization condition: an electrolyte consisting of 0.35 wt% ammonium fluoride+ 2 wt% water + EG, at 30 V.

Table 3. Geometrical Properties of Synthesized TNAs at Various Anodization Time

Properties / Condition	Estimated surface area	Estimated roughness factor	Estimated porosity
Time: 0.5 h	84.48	200.14	0.41
Time: 3 h	205.87	468.39	0.47
Time: 6 h	291.38	655.74	0.49
Time: 9 h	343.89	778.15	0.49
Time: 12 h	401.31	917.68	0.47

are presented in Fig. 5. The effect of anodization voltage experiments was investigated for an electrolyte containing 0.35 wt% of ammonium fluoride, water concentration of 2 wt%, and EG for 3 h under various voltages of 10, 17.5, 25, 35 and 45 volts, followed by calcination at 400 °C for 2 h. Anodization potential crucially affects the nanotube formation and their dimensions, due to the nature of electrochemical anodization process (see, Figs. 2 and 5). Furthermore, the geometrical properties and/or morphological characteristics of as-prepared TNAs were also affected by changing the anodizing voltages, whereby TNAs with different geometries can be synthesized (Table 4). Increasing the supplied potential can increase the hydrolysis of titanium ions and their content in the electrolyte, and also reduces the rate of chemical dissolution, resulted in the formation of longer TNAs.

As shown in Fig. 5a, the photo-electrodes anodized at 17.5, 25, 35 and 45 volts exhibited a tube length of 2.7, 4.4, 10.1 and 13.2 μm, respectively. From Fig. 2i, it can be observed that the fabricated TNAs at 10 V reveals only an amorphous/porous structure, also the experimental data showed that the formation and organization of highly-ordered TNAs at the anodizing voltages below 15 V are very difficult. This phenomenon can be explained by the weak electrochemical etching reaction [36]. As a result, 17 V would be an adequate anodization potential to expand and develop the well-aligned and highly ordered TNAs on titanium sheet. The inner diameter of tubes increased linearly and wall thickness also showed an enhancement with increasing the anodization voltage (Figs. 5b and c).

Longer tubes and larger inner diameter resulted in higher values of SA, G factor and porosity. Photocatalytic performance of the synthesized photoanodes at different anodizing voltages are shown in Fig. 5d, revealing that photocatalytic activity of samples in the terms of degradation of PNP increases with enhancement in applied voltage up to 35 V . This behavior can be attributed to the larger amounts of SA, G factor and porosity of the samples, as listed in Table 4. Lower photocatalytic activity of the anodized sample at 45 V can be explained by limited extinction depth of UV irradiation and diffusion depth of reactants (pollutants) molecules, and higher electron-hole recombination rates of longer tubes [39].

The Effect of Ammonium Fluoride Concentration

According to Eq. (6), NH_4F concentration in electrolyte (to provide fluoride ions) demonstrates a significant effect on the dimensions and morphology of the fabricated TNAs. The experiments related to the impact of NH_4F content were performed using 0.1, 0.2, 0.3 and 0.4 wt% of ammonium fluoride in an electrolyte containing 2 wt% H_2O + ethylene glycol under an applied voltage of 30 V for 3 h, followed by calcinations temperature of 400 °C for 2 h. In the first step (Eq. (5)), surface of titanium foil oxidized electrochemically, and then in the presence of enough water molecules, oxygen ions injected into the body of oxide layer. In the next step, the fluoride ions participated in the field-assisted chemical dissolution reaction and introduced themselves as a key factor to activate the pore drilling [40]. Lack of F^- or existence of disequilibrium reaction between electrochemical oxidation and chemical dissolution of TiO_2 barrier layer caused to appear a sponge-like structure with shorter tubes, as presented in Fig. 2l.

Increase of ammonium fluoride concentration in electrolyte leads to higher chemical dissolution at the oxide/electrolyte interface and faster diffusion rate of fluoride ions from the Ti/TiO_2 interface into the Ti foil, leading the formation of longer tubes (due to attack and migrate of huge number of ions across the barrier layer) [34,41]. As shown in Figs. 6a to c, inner tube diameter and length increased with increment of ammonium fluoride concentration whereas wall thickness shows a little enhancement when NH_4F content increased from 0.1 to 0.4 wt%.

Further increasing of NH_4F concentration in electrolyte causes the collapse of the top tube structures and a significant loss from the pore mouth, resulting in the formation of shorter nanotubes (ammonium fluoride concentration above > 0.45 wt%, not shown in this research) [42]. This behavior is related to the very fast dissolution rate. The best photocatalytic performance was reported for the sample anodized with 0.3 wt% of NH_4F content, due to its better geometrical properties and surface morphology (larger SA and higher G factor), which resulted in more PNP adsorption and then degradation on the TNAs surfaces (Fig. 6d and Table 5).

Generally speaking, photocatalytic performance of the fabricated TNAs *via* anodization method was influenced by

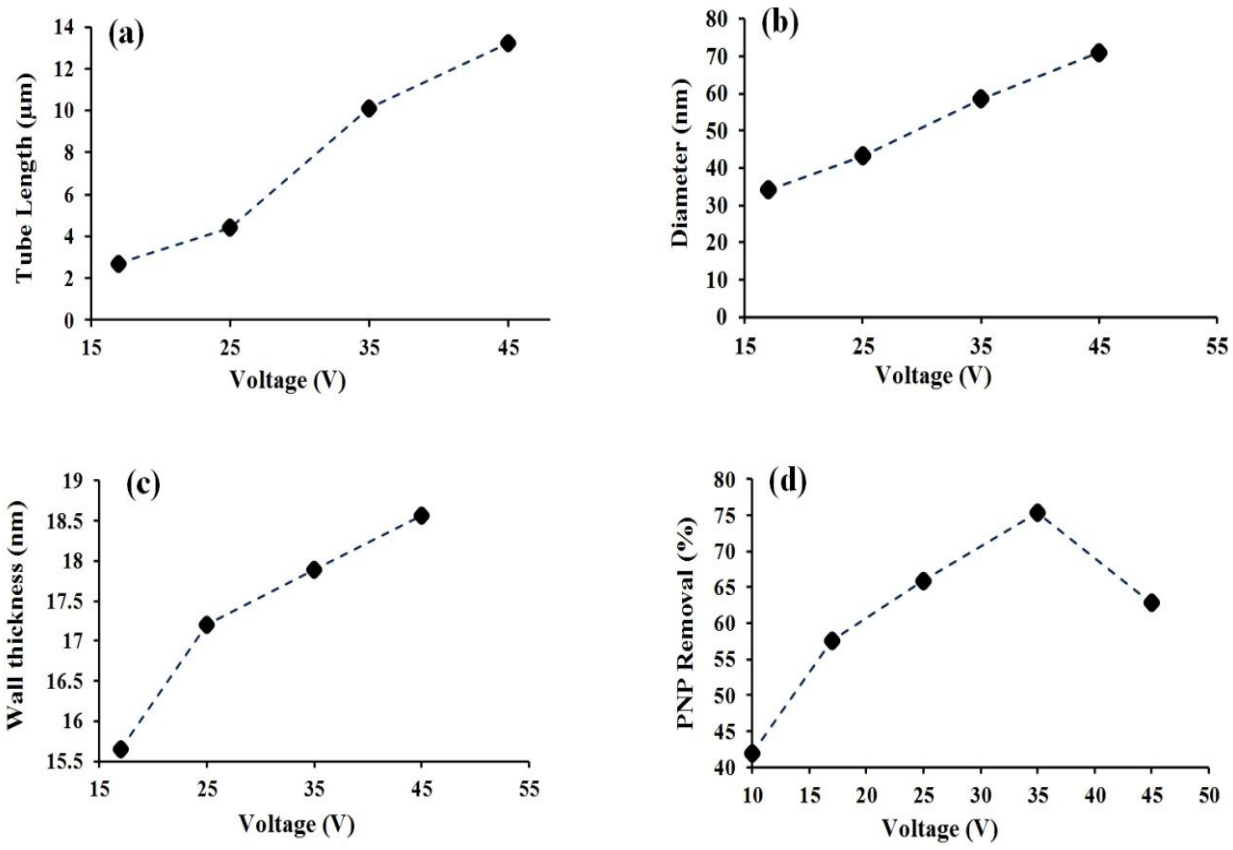

Fig. 5. Influence of anodization potential on length (a), inner diameter (b), wall thickness (c), and PNP photodegradation (d) of TNAs samples which were anodized in an electrolyte including 0.35 wt% NH_4F + 2wt% water + EG for 3 h.

Table 4. Geometrical Properties of Fabricated TNAs at Different Anodizing Voltages

Properties / Condition	Estimated surface area	Estimated roughness factor	Estimated porosity
Voltage: 10 V	N/A[a]	N/A[a]	N/A[a]
Voltage: 17.5 V	88.49	226.15	0.34
Voltage: 25 V	129.48	320.98	0.37
Voltage: 35 V	268.37	629.19	0.44
Voltage: 45 V	323.41	734.46	0.48

[a](N/A): Not applicable, because no nanotubes were formed at this applied voltage.

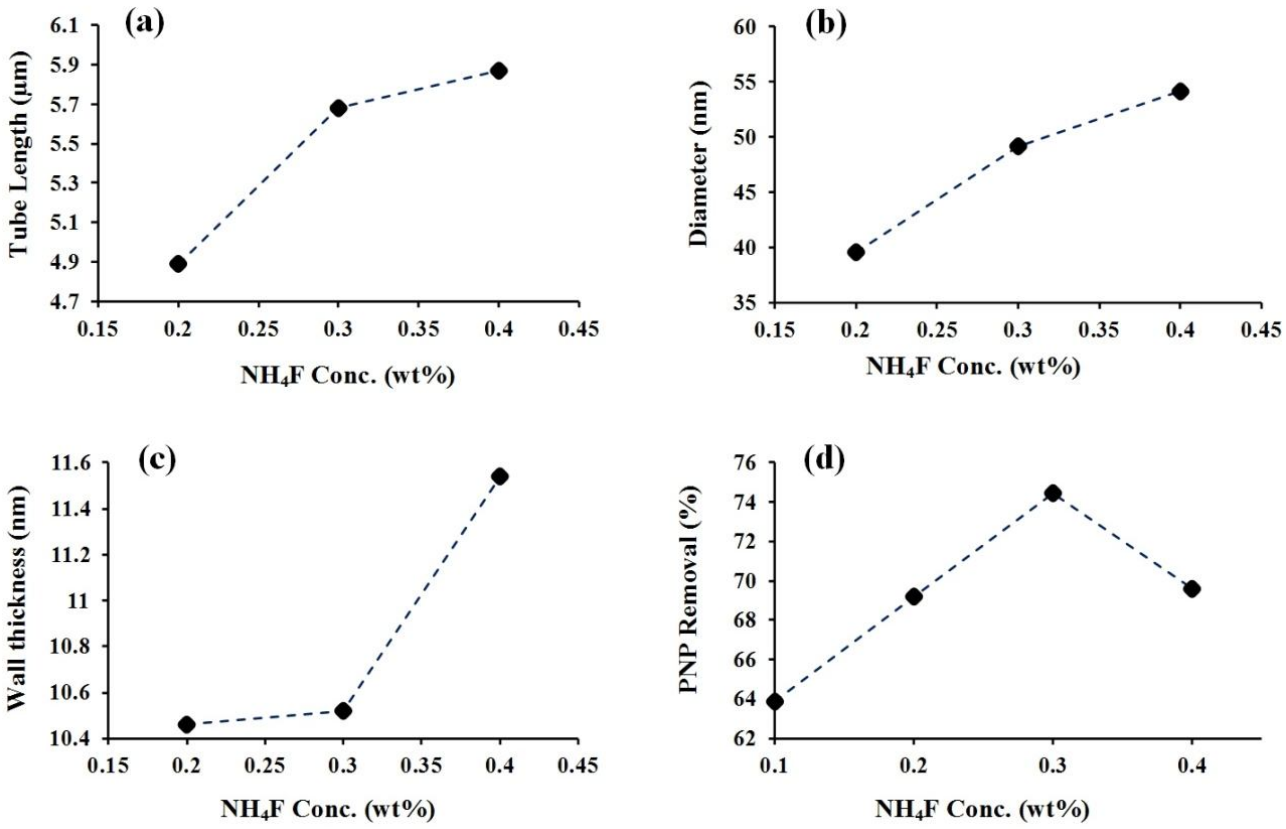

Fig. 6. Influence of ammonium fluoride content in anodizing process on the surface morphology in terms of length (a), inner diameter (b), wall thickness (c) and photocatalytic activity (d) of the samples (anodization condition: an electrolyte containing 2 wt% water + EG, at 30 V and duration time of 3 h).

Table 5. Geometrical properties of the synthesized TNAs using different amounts of ammonium fluoride

Properties / Condition	Estimated surface area	Estimated roughness factor	Estimated porosity
NH_4F Content: 0.1 (wt%)	N/A[a]	N/A[a]	N/A[a]
NH_4F Content: 0.2 (wt%)	214	484.91	0.43
NH_4F Content: 0.3 (wt%)	229	498.81	0.49
NH_4F Content: 0.4 (wt%)	214	468.91	0.50

[a](N/A): Not applicable, because no nanotubes were synthesized at this condition.

their morphological structures in the terms of tube length, diameter and wall thickness. Furthermore, the anodized TNAs with larger active surface area (SA) and G factor can produce more active oxygen species as well as photo-generated electron-hole pairs. Also, the porosity of the synthesized TNAs affected on penetration of reactive molecules (especially oxygen molecules) within nanotubes. Additionally, higher values of SA, G factor and porosity besides thinner wall thickness (due to its restrictive role in the diffusion path for photo-generated electrons and holes) improve the photocatalytic performance of the samples in terms of PNP degradation.

The Effect of Heat Treatment

To investigate the relations between phase transformation (crystallinity) and photo-activity of the fabricated TNAs, annealing treatment varying from 300 to 700 °C was performed. The impact of annealing operation on crystallinity and phot-catalytic performance of various semiconductors has been frequently studied in many different research activities. The annealing treatment was introduced as a beneficial approach to enhance the photo-electrochemical properties of semiconductors. The titanium sheets were first anodized in an ethylene glycol-based electrolyte including 0.38 wt% NH_4F and also 2 wt% H_2O for 4 h, under applied voltage of 40 V, and then calcinations were carried out in the range of 300-700 °C. Figure 7 represents the XRD patterns of annealed TNAs at 400 and 600 °C. Both of XRD patterns reveal the crystalline nature of the photo-anodes and also confirm the presence of anatase phase (JCPDS card No. 00-021-1272), but the phase ratios of anatase/rutile decreased when the calcination temperature increased from 400 °C to 600 °C. The characteristic peaks located at 2θ = 25.4 and 48.16° correspond to the anatase TiO_2 (101) and (200) planes, respectively [13]. Furthermore, two signal diffraction peaks at 27.6° (110) and 36.1° (101) imply the rutile phase in titanium dioxide nanotube arrays (see Fig. 7) [32,36]. With further increment in annealing temperature, intensity of rutile phase increased and also anatase TiO_2 completely transformed into the rutile phase when the samples calcined at temperatures above 750 °C. The experimental X-ray results are consistent with other previous research studies [32,34,36].

As shown in Fig. 8, photocatalytic performance of the samples increases with increasing the annealing temperature up to 500 °C (the sample was mainly composed of anatase TiO_2 with a trace of rutile phase), and then decreases sharply. This behavior is attributed to the formation of rutile phase at temperatures greater than 500 ^oC which consequently accelerates the recombination rate of photogenerated electron-hole and decelerates charge carrier transport [16,43] (see Fig. 8).

CONCLUSIONS

TiO_2 nanotube arrays fabricated by electrochemical anodization of titanium sheet are widely used for applications in many different technical fields such as waste water treatment as a most competitive photocatalyst. The photocatalytic activity of TiO_2 nanotube arrays is directly affected by the anodization parameters. Here, we studied the effects of anodization applied voltage and time, and electrolyte composition, as the key factors, on the surface morphology of the anodized samples including tube length and inner diameter, wall thickness, top-opened or clogged and wall smoothness. The impact of heat treatment (as another independent variable) on phase transformation and photocatalytic performance of the samples were further investigated. A wide range of TNAs dimensions were fabricated at various operating conditions and their photocatalytic performance for PNP degradation under UV-LED irradiation were investigated.

Based on the experimental results, main conclusions are summarized as follows:

- The photo-electrochemical efficiency of the anodized TNAs photoanodes is affected by several independent parameters including electrolyte composition, anodization time, applied voltage, and thermal annealing.
- The morphological and microstructure properties of the fabricated samples, characterized by FE-SEM, reveal that increasing the water content up to 20 wt% affects the length of tubes and their diameter, significantly. Further increase in water content, however, increases the wall thickness, while it has no effect on diameter and tube length. The sample anodized with 1.2 wt% water displays the maximum photocatalytic efficiency of about 74%, due to its higher values of geometrical properties, such as G factor and SA.

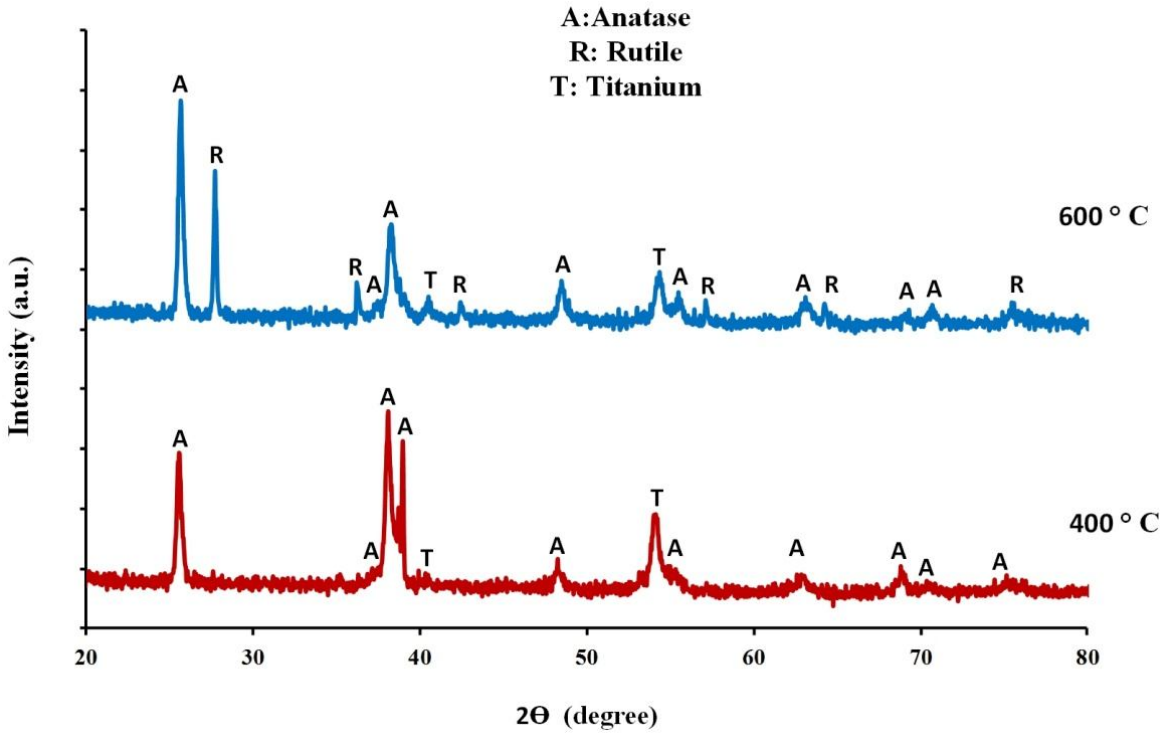

Fig. 7. X-ray diffraction patterns of the synthesized TNAs at different temperatures.

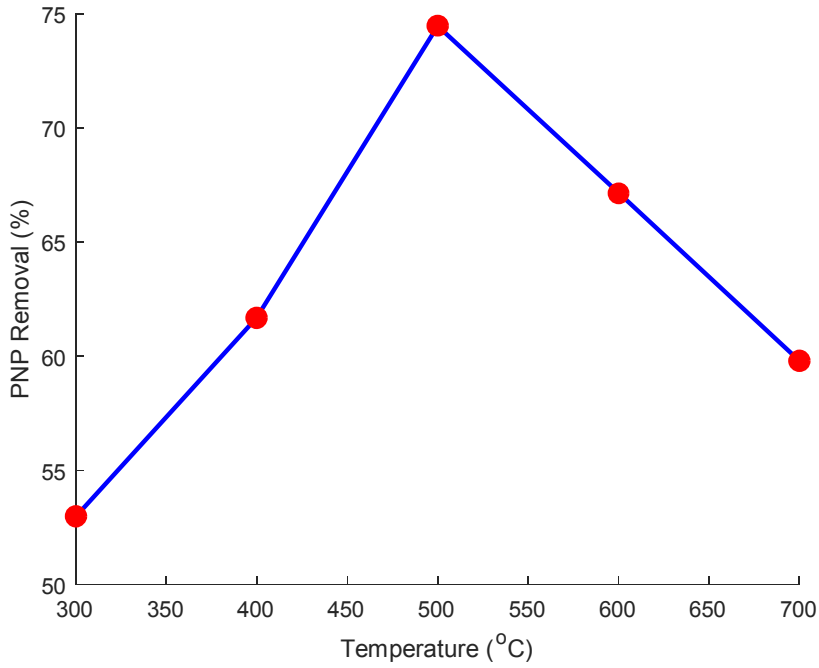

Fig. 8. Influence of heat treatment on photocatalytic performance of TNAs in terms of PNP degradation.

Photocatalytic performance and geometrical properties of the fabricated electrodes decreased with increment of water content in electrolyte.

- Tube length and inner diameter of the anodized samples increase and also wall thickness represents a slightly enhancement by varying of anodization time and applied potential from 0.5 to 12 h and 10 to 45 V, respectively. Photoactivity and geometrical properties of the photoanodes increase with increment of these two key controlling parameters. The highest values of 77% and 75% for PNP degradation reaction were obtained at anodization time and potential of 9 h and 35 V, respectively. Further increase in voltage and duration time decreased the photocatalytic performance of samples, due to the fact that the samples with longer and/or thicker tubes cannot act as an efficient photocatalyst.
- A minimum amount of 0.15 wt% ammonium fluoride is required to organize and form the well-aligned and highly-ordered TNAs. The geometrical characteristics, including SA and G factor, and photoactivity of the fabricated samples, using various amounts of NH_4F, increased up to 0.3 wt% and then slightly decreased. The presence of higher amounts of NH_4F in electrolyte (> 0.45 wt%) destroys the pore mouth and also prevents the tube growth, due to the fast dissolution rate reaction.
- Based on XRD spectra experiments obtained at different annealing temperatures, the heat treatment can significantly change the crystallinity and help to phase transformation. The presence of anatase TiO_2 (as a dominant phase structure) with a small trace of rutile TiO_2 was detected for TNAs sample subjected to heat treatment at 500 °C. Further, the photoanode represented the highest amount of PNP degradation (74.56%) among other annealed samples. Further increase in annealing temperature decreases the anatase to rutile phase ratio and photo-reactivity. This behavior is related to the loss of oxygen in TiO_2 structure that accelerates the recombination rate of photogenerated electron-hole [34,44].

Declarations of Interest

None.

Funding

This research did not receive any specific grant from funding agencies in the public, commercial, or not-for-profit sectors.

REFERENCES

[1] Dsikowitzky, L.; Hagemann, L.; Ariyani, F.; Irianto, H. E.; Schwarzbauer, J., Complex organic pollutant mixtures originating from industrial and municipal emissions in surface waters of the megacity Jakarta-an example of a water pollution problem in emerging economies. *Environ. Sci. Pollut. Res.* **2017**, *24*, 27539-27552. DOI: 10.1007/s11356-017-0164-2.

[2] Salari, H.; Daliri, A.; Gholami, M., Graphitic carbon nitride/reduced graphene oxide/silver oxide nanostructures with enhanced photocatalytic activity in visible light. *Phys. Chem. Res.* **2018**, *6*, 729-740. DOI: 10.22036/PCR.2018.137083.1501.

[3] Salari, H.; Kohantorabi, M., Fabrication of novel Fe_2O_3/MoO_3/AgBr nanocomposites with enhanced photocatalytic activity under visible light irradiation for organic pollutant degradation. *Adv. Powder Technol.* **2020**, *31*, 493-503. DOI: 10.1016/j.apt.2019.11.005.

[4] Salari, H.; Sadeghinia, M., MOF-templated synthesis of nano Ag_2O/ZnO/CuO heterostructure for photocatalysis. *J. Photochem. Photobiol., A* . **2019**, *376*, 279-287. DOI: 10.1016/j.jphotochem.2019.03.010.

[5] Mamaghani, A. H.; Haghighat, F.; Lee, C. -S., Photocatalytic oxidation technology for indoor environment air purification: the state-of-the-art. *Appl. Catal., B.* **2017**, *203*, 247-269. DOI: 10.1016/j.apcatb.2016.10.037.

[6] Bessergenev, V.; Mateus, M.; Morgado, I.; Hantusch, M.; Burkel, E., Photocatalytic reactor, CVD technology of its preparation and water purification from pharmaceutical drugs and agricultural pesticides. *Chem. Eng. J.* **2017**, *312*, 306-316. DOI: 10.1016/j.cej.2016.11.148.

[7] Tsai, C. -Y.; Liu, C. -W.; Chan, Y. H.; Chang, T. -Y.; Chen, B. -C.; Hsi, H. -C., Development of HCl-treated titania nanotube photocatalysts for dye photodegradation and low-concentration elemental mercury removal. *Catal. Today.* **2017**, *297*, 113-123.

DOI: 10.1016/j.cattod.2017.04.061.

[8] Garvey, M.; Panaitescu, E.; Menon, L.; Byrne, C.; Dervin, S.; Hinder, S. J.; *et al*., Titania nanotube photocatalysts for effectively treating waterborne microbial pathogens. *J. Catal.* **2016**, *344*, 631-639. DOI: 10.1016/j.jcat.2016.11.004.

[9] Salari, H., Efficient photocatalytic degradation of environmental pollutant with enhanced photocarrier separation in novel Z-scheme a-MnO_2 nanorod/a-MoO_3 nanocomposites. *J. Photochem. Photobiol., A*. **2020**, *401*, 112787. DOI: 10.1016/j.jphotochem.2020.112787.

[10] Zhang, P.; Song, T.; Wang, T.; Zeng, H., Plasmonic Cu nanoparticle on reduced graphene oxide nanosheet support: An efficient photocatalyst for improvement of near-infrared photocatalytic H_2 evolution. *Appl. Catal., B*. **2018**, *225*, 172-179. DOI: 10.1016/j.apcatb.2017.11.076.

[11] Seifhosseini, M.; Rashidi, F.; Rezaei, M.; Rahimpour, N., Bias potential role in degradation of methyl orange in photocatalytic process. *J. Photochem. Photobiol., A*. **2018**, *360*, 196-203. DOI: 10.1016/j.jphotochem.2018.04.007.

[12] Wang, X.; Zhao, H.; Quan, X.; Zhao, Y.; Chen, S., Visible light photoelectrocatalysis with salicylic acid-modified TiO_2 nanotube array electrode for *p*-nitrophenol degradation. *J. Hazard. Mater.* **2009**, *166*, 547-552. DOI: 10.1016/j.jhazmat.2008.11.066.

[13] Mollavali, M.; Falamaki, C.; Rohani, S., Preparation of multiple-doped TiO_2 nanotube arrays with nitrogen, carbon and nickel with enhanced visible light photoelectrochemical activity *via* single-step anodization. *Int. J. Hydrogen Energy.* **2015**, *40*, 12239-12252. DOI: 10.1016/j.ijhydene.2015.07.069.

[14] Gholami, M.; Qorbani, M.; Moradlou, O.; Naseri, N.; Moshfegh, A. Z., Optimal Ag_2S nanoparticle incorporated TiO2 nanotube array for visible water splitting. *RSC Adv.* **2014**, *4*, 7838-7844. DOI: 10.1039/c3ra44898c.

[15] Raja, K.; Gandhi, T.; Misra. M., Effect of water content of ethylene glycol as electrolyte for synthesis of ordered titania nanotubes. *Electrochem. Commun.* **2007**, *9*, 1069-1076. DOI: 10.1016/j.elecom.2006.12.024.

[16] Wan, J.; Yan, X.; Ding, J.; Wang, M.; Hu, K., Self-organized highly ordered TiO_2 nanotubes in organic aqueous system. *Mater. Charact.* **2009**, *60*, 1534-1540. DOI: 10.1016/j.matchar.2009.09.002.

[17] Vaenas, N.; Bidikoudi, M.; Stergiopoulos, T.; Likodimos, V.; Kontos, A. G.; Falaras, P., Annealing effects on self-assembled TiO_2 nanotubes and their behavior as photoelectrodes in dye-sensitized solar cells. *Chem. Eng. J.* **2013**, *224*, 121-127. DOI: 10.1016/j.cej.2013.02.017.

[18] Thabit, M.; Liu, H.; Zhang, J.; Wang, B., Fabrication of titanium dioxide nanotube photo-electrodes in different electrolyte mixtures and the impacts on their characteristics and photo-catalytic abilities under visible light. *Pol. J. Chem. Technol.* **2017**, *19*, 34-40. DOI: 10.1515/pjct-2017-0005.

[19] Chernozem, R. V.; Surmeneva, M. A.; Surmenev, R. A., Influence of anodization time and voltage on the parameters of TiO_2 nanotubes. *IOP Conf. Ser. Mater. Sci. Eng.* **2016**. *116*. 012025. DOI: 10.1088/1757-899x/116/1/012025.

[20] Sulka, G. D.; Kapusta-Kołodziej, J.; Brzózka, A.; Jaskuła, M., Anodic growth of TiO_2 nanopore arrays at various temperatures. *Electrochim. Acta.* **2013**, *104*, 526-535. DOI: 10.1016/j.electacta.2012.12.121.

[21] Sun, Y.; Zhao, Q.; Wang, G.; Yan, K., Influence of water content on the formation of TiO_2 nanotubes and photoelectrochemical hydrogen generation. *J. Alloys Compd.* **2017**, *711*, 514-520. DOI: 10.1016/j.jallcom.2017.03.007.

[22] Song, H.; Cheng, K.; Guo, H.; Wang, F.; Wang, J.; Zhu, N.; *et al.*, Effect of ethylene glycol concentration on the morphology and catalytic properties of TiO_2 nanotubes. *Catal. Commun.* **2017**, *97*, 23-26. DOI: 10.1016/j.catcom.2017.04.005.

[23] Hou, Y.; Li, X.; Zhao, Q.; Quan, X.; Chen, G., Electrochemically assisted photocatalytic degradation of 4-chlorophenol by $ZnFe_2O_4$-modified TiO_2 nanotube array electrode under visible light irradiation. *Environ. Sci. Technol.* **2010**, *44*, 5098-5103. DOI: 10.1021/es100004u.

[24] Feng, H.; Chen, L.; Yuan, L.; Cai, Q., Visible light-induced efficiently oxidative decomposition of *p*-Nitrophenol by CdTe/TiO_2 nanotube arrays. *Chem.*

Eng. J. **2013**, 215, 591-599. DOI: 10.1016/j.cej.2012.11.044.

[25] Noeiaghaei, T.; Yun, J.-H.; Nam, S.; Zoh, K.; Gomes, V.; Kim. J.; *et al.*, The influence of geometrical characteristics on the photocatalytic activity of TiO_2 nanotube arrays for degradation of refractory organic pollutants in wastewater. *Water Sci. Technol.* **2015**, *71*, 1301-1309. DOI: 10.2166/wst.2015.078.

[26] Kontos, A.; Kontos, A.; Tsoukleris, D.; Likodimos, V.; Kunze, J.; Schmuki, P.; *et al.*, Photo-induced effects on self-organized TiO_2 nanotube arrays: the influence of surface morphology. *Nanotechnol.* **2008**, *20*, 045603. DOI: 10.1088/0957-4484/20/4/045603.

[27] Kontos, A.; Katsanaki, A.; Maggos, T.; Likodimos, V.; Ghicov, A.; Kim, D.; *et al.* Photocatalytic degradation of gas pollutants on self-assembled titania nanotubes. *Chem. Phys. Lett.* **2010**, *490*, 58-62. DOI: 10.1016/j.cplett.2010.03.009.

[28] Zhu, K.; Neale, N. R.; Miedaner, A.; Frank, A. J., Enhanced charge-collection efficiencies and light scattering in dye-sensitized solar cells using oriented TiO_2 nanotubes arrays. *Nano Lett.* **2007**, *7*, 69-74. DOI: 10.1021/nl062000o.

[29] Li, T.; Luo, S.; Yang, L., Microwave-assisted solvothermal synthesis of flower-like Ag/AgBr/BiOBr microspheres and their high efficient photocatalytic degradation for p-nitrophenol. *J. Solid State Chem.* **2013**, *206*, 308-316. DOI: 10.1016/j.jssc.2013.07.019

[30] Mor, G. K.; Varghese, O. K.; Paulose, M.; Shankar, K.; Grimes, C. A., A review on highly ordered, vertically oriented TiO_2 nanotube arrays: Fabrication, material properties, and solar energy applications. *Sol. Energy Mater. Sol. Cells.* **2006**, *90*, 2011-2075. DOI: 10.1016/j.solmat.2006.04.007.

[31] Mollavali, M.; Falamaki, C.; Rohani, S., Efficient light harvesting by NiS/CdS/ZnS NPs incorporated in C, N-co-doped-TiO_2 nanotube arrays as visible-light sensitive multilayer photoanode for solar applications. *Int. J. Hydrogen Energy.* **2018**, *43*, 9259-9278. DOI: 10.1016/j.ijhydene.2018.03.102.

[32] Li, Y.; Yu, H.; Zhang, C.; Song, W.; Li, G.; Shao, Z.; *et al.*, Effect of water and annealing temperature of anodized TiO_2 nanotubes on hydrogen production in photoelectrochemical cell. *Electrochim. Acta.* **2013**, *107*, 313-319. DOI: 10.1016/j.electacta.2013.05.090.

[33] Yoriya, S.; Paulose, M.; Varghese, O. K.; Mor, G. K.; Grimes, C. A., Fabrication of vertically oriented TiO_2 nanotube arrays using dimethyl sulfoxide electrolytes. *J. Phys. Chem. C.* **2007**, *111*, 13770-13776. DOI: 10.1021/jp074655z.

[34] Matsuda, A.; Sreekantan, S.; Krengvirat, W., Well-aligned TiO_2 nanotube arrays for energy-related applications under solar irradiation. *J. Asian Ceram. Soc.* **2013**, *1*, 203-219. DOI: 10.1016/j.jascer.2013.07.001.

[35] Sulka, G. D.; Kapusta-Kołodziej, J.; Brzózka, A.; Jaskuła, M., Fabrication of nanoporous TiO_2 by electrochemical anodization. *Electrochim. Acta.* **2010**, *55*, 4359-4367. DOI: 10.1016/j.electacta.2009.12.053.

[36] Liang, H. C.; Li, X. Z., Effects of structure of anodic TiO_2 nanotube arrays on photocatalytic activity for the degradation of 2,3-dichlorophenol in aqueous solution. *J. Hazard. Mater.* **2009**, *162*, 1415-1422. DOI: 10.1016/j.jhazmat.2008.06.033.

[37] Macak, J. M.; Schmuki, P., Anodic growth of self-organized anodic TiO_2 nanotubes in viscous electrolytes. *Electrochim. Acta.* **2006**, *52*, 1258-1264. DOI: 10.1016/j.electacta.2006.07.021.

[38] Yun, J. -H., Ng, Y. H.; Ye, C.; Mozer, A. J.; Wallace, G. G.; Amal, R., Sodium fluoride-assisted modulation of anodized TiO_2 nanotube for dye-sensitized solar cells application. *ACS Appl. Mater. Interfaces.* **2011**, *3*, 1585-1593. DOI: 10.1021/am200147b.

[39] Nischk, M.; Mazierski, P.; Gazda, M.; Zaleska, A., Ordered TiO2 nanotubes: The effect of preparation parameters on the photocatalytic activity in air purification process. *Appl. Catal., B.* **2014**, *144*, 674-685. DOI: 10.1016/j.apcatb.2013.07.041.

[40] Ku, Y.; Chen, Y. -S.; Hou, W. -M.; Chou, Y. -C., Effect of NH_4F concentration in electrolyte on the fabrication of TiO_2 nanotube arrays prepared by anodisation. *Micro Nano Lett.* **2012**, *7*, 939-942. DOI: 10.1049/mnl.2012.0488.

[41] Xue, Y.; Sun, Y.; Wang, G.; Yan, K.; Zhao, J., Effect of NH_4F concentration and controlled-charge consumption on the photocatalytic hydrogen generation of TiO_2 nanotube arrays. *Electrochim.*

Acta. **2015**, *155*, 312-320. DOI: 10.1016/j.electacta.2014.12.134.

[42] Xie, Z.; Blackwood, D., Effects of anodization parameters on the formation of titania nanotubes in ethylene glycol. *Electrochim. Acta*. **2010**, *56*, 905-912. DOI: 10.1016/j.electacta.2010.10.004.

[43] Li, H.; Cao, L.; Liu, W.; Su, G.; Dong, B., Synthesis and investigation of TiO_2 nanotube arrays prepared by anodization and their photocatalytic activity. *Ceram. Int.* **2012**, *38*, 5791-5797. DOI: 10.1016/j.ceramint.2012.04.026.

[44] Salari, M.; Konstantinov, K.; Liu, H. K., Enhancement of the capacitance in TiO_2 nanotubes through controlled introduction of oxygen vacancies. *J. Mater. Chem.*. **2011**, *21*, 5128-5133. DOI: 10.1039/c0jm04085a.